

University of Nebraska - Lincoln

DigitalCommons@University of Nebraska - Lincoln

Publications from USDA-ARS / UNL Faculty

U.S. Department of Agriculture: Agricultural
Research Service, Lincoln, Nebraska

1-1-2023

Modeling Perennial Bioenergy Crops in the E3SM Land Model (ELMv2)

Eva Sinha

Pacific Northwest National Laboratory

Katherine V. Calvin

Pacific Northwest National Laboratory

Ben Bond-Lamberty

Pacific Northwest National Laboratory

Beth A. Drewniak

Argonne National Laboratory

Daniel M. Ricciuto

Oak Ridge National Laboratory

See next page for additional authors

Follow this and additional works at: <https://digitalcommons.unl.edu/usdaarsfacpub>



Part of the [Agriculture Commons](#)

Sinha, Eva; Calvin, Katherine V.; Bond-Lamberty, Ben; Drewniak, Beth A.; Ricciuto, Daniel M.; Sargsyan, Khachik; Cheng, Yanyan; Bernacchi, Carl; and Moore, Caitlin E., "Modeling Perennial Bioenergy Crops in the E3SM Land Model (ELMv2)" (2023). *Publications from USDA-ARS / UNL Faculty*. 2591.
<https://digitalcommons.unl.edu/usdaarsfacpub/2591>

This Article is brought to you for free and open access by the U.S. Department of Agriculture: Agricultural Research Service, Lincoln, Nebraska at DigitalCommons@University of Nebraska - Lincoln. It has been accepted for inclusion in Publications from USDA-ARS / UNL Faculty by an authorized administrator of DigitalCommons@University of Nebraska - Lincoln.

Authors

Eva Sinha, Katherine V. Calvin, Ben Bond-Lamberty, Beth A. Drewniak, Daniel M. Ricciuto, Khachik Sargsyan, Yanyan Cheng, Carl Bernacchi, and Caitlin E. Moore












RESEARCH ARTICLE

10.1029/2022MS003171

Modeling Perennial Bioenergy Crops in the E3SM Land Model (ELMv2)

Key Points:

- The study expands the Energy Exascale Earth System Land Model to include perennial bioenergy crops miscanthus and switchgrass
- Calibrated model captures the observed seasonality and the magnitude of carbon and energy fluxes
- This study provides the foundation for future research examining the impact of perennial bioenergy crop expansion

Eva Sinha¹ , Katherine V. Calvin² , Ben Bond-Lamberty² , Beth A. Drewniak³ , Daniel M. Ricciuto⁴ , Khachik Sargsyan⁵ , Yanyan Cheng^{1,6} , Carl Bernacchi^{7,8} , and Caitlin E. Moore^{8,9} 

¹Pacific Northwest National Laboratory, Richland, WA, USA, ²Joint Global Change Research Institute, Pacific Northwest National Laboratory, College Park, MD, USA, ³Argonne National Laboratory, Lemont, IL, USA, ⁴Oak Ridge National Laboratory, Oak Ridge, TN, USA, ⁵Sandia National Laboratories, Livermore, CA, USA, ⁶Department of Industrial Systems Engineering and Management, National University of Singapore, Singapore, Singapore, ⁷Global Change and Photosynthesis Research Unit, USDA-ARS, Urbana, IL, USA, ⁸University of Illinois at Urbana-Champaign, Urbana, IL, USA, ⁹School of Agriculture and Environment, The University of Western Australia, Crawley, WA, Australia

Supporting Information:

Supporting Information may be found in the online version of this article.

Correspondence to:

E. Sinha,
eva.sinha@pnnl.gov

Citation:

Sinha, E., Calvin, K. V., Bond-Lamberty, B., Drewniak, B. A., Ricciuto, D. M., Sargsyan, K., et al. (2023). Modeling perennial bioenergy crops in the E3SM land model (ELMv2). *Journal of Advances in Modeling Earth Systems*, 15, e2022MS003171. <https://doi.org/10.1029/2022MS003171>

Received 3 MAY 2022
Accepted 21 DEC 2022

Author Contributions:

Conceptualization: Eva Sinha, Katherine V. Calvin, Ben Bond-Lamberty
Data curation: Carl Bernacchi, Caitlin E. Moore
Formal analysis: Eva Sinha
Investigation: Eva Sinha
Methodology: Eva Sinha, Daniel M. Ricciuto, Khachik Sargsyan
Resources: Eva Sinha

Abstract Perennial bioenergy crops are increasingly important for the production of ethanol and other renewable fuels, and as part of an agricultural system that alters the climate through its impact on biogeophysical and biogeochemical properties of the terrestrial ecosystem. Few Earth System Models (ESMs) represent such crops, however. In this study, we expand the Energy Exascale Earth System Land Model to include perennial bioenergy crops with a high potential for mitigating climate change. We focus on high-productivity miscanthus and switchgrass, estimating various parameters associated with their different growth stages and performing a global sensitivity analysis to identify and optimize these parameters. The sensitivity analysis identifies five parameters associated with phenology, carbon/nitrogen allocation, stomatal conductance, and maintenance respiration as the most sensitive parameters for carbon and energy fluxes. We calibrated and validated the model against observations and found that the model closely captures the observed seasonality and the magnitude of carbon fluxes. The validated model represents the latent heat flux fairly well, but sensible heat flux for miscanthus is not well captured. Finally, we validated the model against observed leaf area index (LAI) and harvest amount and found modeled LAI captured observed seasonality, although the model underestimates LAI and harvest amount. This work provides a foundation for future ESM analyses of the interactions between perennial bioenergy crops and carbon, water, and energy dynamics in the larger Earth system, and sets the stage for studying the impact of future biofuel expansion on climate and terrestrial systems.

Plain Language Summary Perennial bioenergy crops are not well represented in global land models, despite projected increase in their production. Our study expands Energy Exascale Earth System Land Model to include perennial bioenergy crops and calibrates the model for miscanthus and switchgrass. The calibrated model captures the seasonality and magnitude of carbon and energy fluxes. This study provides the foundation for future research examining the impact of perennial bioenergy crop expansion.

1. Introduction

Cropland occupies 11% of the global land (FAO, 2021; Klein Goldewijk et al., 2017) and can alter the regional and global climate through biogeochemical and biophysical impacts on the land surface (D. L. Lombardozzi et al., 2020; Seguin et al., 2007). Examples of biogeochemical impacts include large increase in CO₂ emissions resulting from the replacement of native vegetation with cropland (Fargione et al., 2008; Seguin et al., 2007). Although increased agricultural productivity results in enhanced CO₂ uptake during the growing season, different management practices can result in net increase in CO₂ and other greenhouse gas emissions such as methane and nitrous oxide (Searchinger et al., 2008; Verge et al., 2007). The biophysical impacts on the land surface include modification of the surface energy and water budget. For example, agricultural intensification and the resulting increase in evapotranspiration causes a decrease in extreme summer temperature and an increase in precipitation (Mueller et al., 2016) while the use of cover crops impacts regional temperature and causes warmer winters (D. Lombardozzi et al., 2018).

Earth System Models (ESMs) that are used for climate projections should have adequate representation of crops due to the impact of agriculture on regional and global climate. However, most ESMs represent crops

Software: Eva Sinha, Daniel M. Ricciuto, Khachik Sargsyan
Supervision: Katherine V. Calvin, Ben Bond-Lamberty, Beth A. Drewniak
Validation: Eva Sinha
Visualization: Eva Sinha
Writing – original draft: Eva Sinha
Writing – review & editing: Eva Sinha, Katherine V. Calvin, Ben Bond-Lamberty, Beth A. Drewniak, Daniel M. Ricciuto, Khachik Sargsyan, Yanyan Cheng, Carl Bernacchi, Caitlin E. Moore

as generic-grass that fails to capture the various phenological phases of crops and differences across various crop species (Levis, 2010; McDermid et al., 2017; Moore et al., 2021). This simplistic representation of crops underestimates gross primary productivity and latent heat flux from agricultural regions (D. L. Lombardozzi et al., 2020). To address this shortcoming and to improve the simulation of carbon and water fluxes, several land model components of ESMs are now simulating major crops, including the Community Land Model (Drewniak et al., 2013; Levis et al., 2012), E3SM land model (Golaz et al., 2022), Joint UK Land Environment Simulator (JULES) (Osborne et al., 2015), Noah-MP-Crop (Liu et al., 2016), Organizing Carbon and Hydrology In Dynamic Ecosystems (ORCHIDEE) (Wu et al., 2016), and Simple Biosphere Model (Lokupitiya et al., 2009).

Perennial bioenergy crops are however not well represented in ESMs, despite large increases in bioenergy production projected in modeled socioeconomic pathways for meeting future energy demands and for mitigating climate change. Energy crops are expected to account for a significant portion of bioenergy in the U.S. by 2040 (Langholtz et al., 2016). The quantity of bioenergy production required in the future is highly uncertain and will depend on the future energy demand and radiative forcing level, among other factors. For example, it is estimated that to limit future warming to 1.5°C, 40–310 EJ yr⁻¹ of bioenergy will be required (IPCC, 2018). Another study estimates future land area required for bioenergy production to range between 120 and 470 million ha for the RCP4.5 mitigation scenario and between 250 and 1,500 million ha for the RCP2.6 mitigation scenario (Popp et al., 2017). To understand the impact of such increased biomass production on carbon, water, and energy fluxes, perennial bioenergy crops should be adequately represented in ESMs including optimizing various crop parameters and quantifying the parametric uncertainty. This has been achieved in select land components of ESMs. For example, Song et al. (2015) incorporated *Miscanthus × giganteus* (miscanthus) and two different varieties of switchgrass in Integrated Science Assessment Model and used it to study the spatial and temporal patterns in biomass yield in the eastern United States. Zhu et al. (2017) parameterized and validated Community Land Model (CLM) version 4.5 for miscanthus and switchgrass and estimated carbon and surface energy balance from the growth of these crops across the Continental United States. Li, Yue, et al. (2018) implemented four major perennial bioenergy crops in the global dynamic vegetation model, ORCHIDEE, and utilized it to compare simulated versus observed biomass yield. Cheng et al. (2020) incorporated two perennial bioenergy crops into CLM version 5 and found that compared to traditional bioenergy crops, perennial crops have higher carbon uptake and lower nutrient requirement that increases their suitability for future bioenergy production. Littleton et al. (2020) modified JULES land surface model to simulate the growth and harvest of perennial bioenergy crops and applied the updated model for estimating global annual yield of miscanthus under the future climate.

Comprehensively calibrating ESMs crop parameters poses a significant challenge due to the large number of parameters and considerable computational cost of calibration. ESMs simulate various terrestrial and biogeochemical processes by utilizing a vast array of parameters that can contribute large uncertainties in model predictions (Lambert et al., 2013; Qian et al., 2018). The ESM crop-models often use default global parameter values rather than region-specific values that results in large biases between model simulated and observed fluxes (Cheng et al., 2021). These biases can be reduced by calibrating the model and finding the optimal parameter ranges (Lu et al., 2018). Model calibration is often preceded by sensitivity analysis for identifying the most influential parameters for various model outputs (Ricciuto et al., 2018). However, model complexity and long simulation time required for achieving biogeochemical equilibrium makes sensitivity analysis and calibration computationally expensive. These challenges have caused several studies to either modify the crop parameters based on values in literature or field observations (Boas et al., 2021; Li, Yue, et al., 2018; Zhu et al., 2017), or to calibrate the model by utilizing one-at-time approach that varies a single model parameter at a time (Cheng et al., 2020; Littleton et al., 2020; Song et al., 2013, 2015). However, both these approaches fail to account for the impact of joint parameter variability on model outputs (Qian et al., 2018; Ricciuto et al., 2018). To overcome these challenges, studies are now constructing ESM surrogates followed up by global sensitivity analysis (GSA) and model calibration using these surrogates (Lu & Ricciuto, 2019; Lu et al., 2018; Ricciuto et al., 2018).

The objective of this study is to expand the crop modeling capability of the Energy Exascale Earth System Model (E3SM) land component (ELMv2) to include perennial crops that have phenological stages distinct from annual crops. The expanded crop model is parameterized for two perennial bioenergy crops—miscanthus (*Miscanthus × giganteus*) and switchgrass (*Panicum virgatum* L.). The model parameterization is achieved by calibrating simulated carbon and energy fluxes that is performed by developing ELM surrogates, conducting a GSA, and carrying out Bayesian calibration using carbon and energy flux measurements. The model is validated by utilizing leaf area index (LAI) and harvest measurements.

2. Model Development

The E3SM land model version 2 (ELMv2) is branched from CLM version 4.5 (CLM4.5) (Oleson et al., 2013). Major additions to ELM since diverging from CLM4.5 include improved representation of atmospheric aerosols, a minor bug fix in evaporation estimation from permeable surfaces, an updated scheme for calculation of leaf stomatal conductance, and modification to the nighttime albedo calculation. These differences between ELM and CLM4.5 are described in more detail in Golaz et al. (2019), Burrows et al. (2020), and Ricciuto et al. (2018). For capturing the impact of agriculture on climate and vice-versa, ELM includes representation of annual crops, maize, soybean, and spring wheat in its crop model (Drewniak et al., 2013; Levis et al., 2012). Recent updates to the crop model include the implementation of dynamic root modeling (Drewniak, 2019) and climate driven planting date estimation. The crop models in both CLM4.5 and ELM do not include representation of perennial crops. Perennial crops are distinctly different from annual crops. For example, differences in albedo and rooting depth result in increased evapotranspiration in perennial crops that can have a cooling effect (Georgescu et al., 2011). Additionally, perennial crops such as miscanthus and switchgrass require fewer fertilizer inputs and reduce nitrogen leaching compared with maize and soybean (Smith et al., 2013). As such, fertilizer was applied to both bioenergy crops after crop emergence at the default rate of 84 kg ha⁻¹ yr⁻¹ over a period of 20 days to maximize nitrogen utilization by plants and minimize nitrogen loss through denitrification. This study implements perennial crop modeling in ELM and the subsections below describe the phenology, carbon and nitrogen allocation, and harvest for perennial crops.

2.1. Phenology

The perennial crop phenology consisted of three distinct phases: crop emergence, leaf onset, and leaf senescence. The perennial crops are planted once and the crops re-grow from underground lignotubers each year. In ELM, the crop plantation in the first year and re-emergence in the following years occurs between the minimum and maximum plant emergence date when the temperature thresholds are met (Equations 1–3).

$$T_{10d} < \bar{T}_p \quad (1)$$

$$T_{10d}^{\min} < \bar{T}_p^{\min} \quad (2)$$

$$\bar{d}_{plant}^{\min} \leq jday \leq \bar{d}_{plant}^{\max} \quad (3)$$

where T_{10d} is the 10-day running mean of T_{2m} (the simulated 2-m air temperature during each model time step) and T_{10d}^{\min} is the 10-day running mean of T_{2m}^{\min} (the daily minimum of T_{2m}). \bar{T}_p and \bar{T}_p^{\min} are crop-specific coldest plant emergence temperatures. \bar{d}_{plant}^{\min} and \bar{d}_{plant}^{\max} are the crop-specific minimum and maximum plant emergence date, respectively, and $jday$ is the Julian day. All variables with an accent bar are model parameters and ones without an accent bar are model estimated values. The \bar{T}_p^{\min} parameter was set to 273.15 K and \bar{d}_{plant}^{\min} and \bar{d}_{plant}^{\max} parameters were set to 1 March and 1 May, respectively for both miscanthus and switchgrass.

The leaf onset starts when the growing degree days (GDDs) accumulated (Equation 4) since plant emergence exceeds the crop-specific minimum GDD requirement (Equation 5).

$$GDD^n = GDD^{n-1} + (T_{s,3} - T_{frz}) \times f_{day} \quad (4)$$

$$GDD^n = \overline{GDD}^{\min} \quad (5)$$

where GDD^n is the GDD accumulated at time step n (°day), $T_{s,3}$ is the temperature of the third soil layer (K), T_{frz} is the freezing point of water (273.15 K), f_{day} is the model time step (day), \overline{GDD}^{\min} is the minimum GDD requirement (°day).

The leaf senescence occurs when the temperature and leaf age criteria are met (Equations 6–7).

$$T_{10d} < \bar{T}_s \quad (6)$$

$$n_{days\ on} > \bar{n}_{min} \quad (7)$$

where \bar{T}_s is the crop-specific senescence temperature, $n_{days\ on}$ is the leaf age in days, and \bar{n}_{min} is the crop-specific minimum leaf age.

2.2. C and N Allocation

Similar to the annual crops being modeled in ELM, carbon and nitrogen assimilation in the perennial crops is based on phenological stages. The carbon/nitrogen (CN) allocation is simulated throughout the growing period; starting in the leaves, stem, and fine roots with leaf emergence, and ending at the time of the harvest. The CN ratios in the leaf, stem, and roots vary all through the growth period and are modeled based on CLM4.5 carbon and nitrogen allocation scheme (Oleson et al., 2013). Time varying allocation coefficients are used for estimating the fraction of carbon that is assigned to the leaf, stem, and fine roots (Equations 8–10). These coefficients are similar to the allocation coefficients used for annual crop phase between leaf emergence and grain fill. The stem and fine root coefficients are the same as the annual crop coefficients while the leaf coefficient has \overline{GDD}_{mat} (GDDs required for maturity) replacing the heat unit index of the annual crops.

$$a_{froot} = \bar{a}_{froot}^i - \left(\bar{a}_{froot}^i - \bar{a}_{froot}^f \right) \frac{GDD_{T2m}}{\overline{GDD}_{mat}} \quad \text{where} \quad \frac{GDD_{T2m}}{\overline{GDD}_{mat}} \leq 1 \quad (8)$$

$$a_{leaf} = (1 - a_{froot}) \frac{\bar{a}_{leaf}^i \left(e^{-\bar{b}} - e^{-\bar{b} \frac{GDD_{T2m}}{\overline{GDD}_{mat}}} \right)}{e^{-\bar{b}} - 1} \quad (9)$$

$$a_{livestem} = 1 - a_{froot} - a_{leaf} \quad (10)$$

where, \bar{a}_{froot}^i , \bar{a}_{froot}^f , and \bar{a}_{leaf}^i are initial and final values of root and leaf carbon allocation coefficients. \bar{b} is an exponential factor used in leaf carbon allocation, \overline{GDD}_{mat} is the GDD required for the crop to reach maturity, and GDD_{T2m} is the GDD for 2m air temperature.

2.3. Harvest

The perennial crop harvest occurs as soon as the leaf senescence (Equations 6–7) criteria are met. During harvest, most of the C and N stored in above-ground biomass comprised of leaf and live stem are removed. To account for maximum conversion of above-ground biomass to harvest, 95% of the available C and N is converted for food/biofuel production and the remainder is transferred to the litter pool. This removal rate is higher than the 70% removal rate considered in CLM (Cheng et al., 2020; Zhu et al., 2017). The carbon content of harvested biomass is divided by 0.447 to convert it to harvest yield (Zeri et al., 2013).

3. Model Evaluation

In order to identify the impact of model parameters on output quantities of interests (QoIs), as well as to quantify and reduce predictive variance associated with these uncertain parameters, we will first construct a surrogate approximation of the model across a range of variability of the parameters, followed by GSA, and Bayesian calibration of this pre-constructed surrogate.

3.1. Model Simulation and Surrogate Construction

A total of 20 perennial crop parameters related to crop phenology, CN allocation, and photosynthetic capacity were selected for the surrogate construction, GSA and model calibration (Table 1). We identified the input range for these parameters through literature review. If an input range for a parameter was not available in the literature then it was set based on expert judgment. The 20 parameters were randomly varied within their input range for 2,000 ELM simulations. We used the Offline Land Model Testbed (Ricciuto, 2022) for 2,000 ensemble ELM runs, each of which ran for 200 years in the accelerated spin-up mode and 200 years in the non-accelerated

Table 1
Descriptions, Input Ranges, and Sources of Information Used for the 20 Input Parameters Varied in This Study

Parameter	ELM variable	Units	Description	Minimum	Maximum	Source
\bar{T}_p	planting_temp	K	Average 10-day temperature required for plant emergence	275	285	1
\overline{GDD}^{\min}	gddmin	°day	Minimum growing degree days	50	320	2
\bar{T}_s	senescence_temp	K	Average 10-day temperature for leaf senescence	280	290	1
\bar{n}_{\min}	min_days_senes	days	Minimum leaf age to allow for leaf senescence	90	120	3
\bar{a}_{froot}^i	arooti	–	Root CN allocation coefficient	0.05	0.3	4
\bar{a}_{froot}^f	arootf	–	Root CN allocation coefficient	0.05	0.2	4
\bar{a}_{leaf}^i	fleafi	–	Leaf CN allocation coefficient	0.5	0.95	4
\bar{b}	bfact	–	Exponential factor for leaf CN allocation	0.05	0.15	2
\overline{GDD}_{mat}	hybgdd	°day	Growing degree days required for maturity	1,600	2,000	2
	leafcn	gC gN ⁻¹	Leaf CN ratio	15	35	2
	livewdcn	gC gN ⁻¹	Live wood CN ratio	40	60	2
	frootcn	gC gN ⁻¹	Fine root CN ratio	20	50	5
	graincn	gC gN ⁻¹	Grain CN ratio	25	60	6
	laimx	–	Maximum leaf area index used in CNVegStructUpdate	5	12	4
	slatop	m ² gC ⁻¹	Specific leaf area (SLA) at top of canopy, projected area basis	0.01	0.07	4
	i_vc	umol CO ₂ m ⁻² s ⁻¹	Intercept of the relationship between leaf N per unit area and V_{cmax}	3	35	4
	s_vc	umol CO ₂ m ⁻² s ⁻¹	Slope of the relationship between leaf N per unit area and V_{cmax}	6	70	4
	br_mr	umol CO ₂ m ⁻² s ⁻¹	Base rate for maintenance respiration (MR)	1.26E–06	3.75E–06	7
	q10_mr	–	Temperature sensitivity for MR	1.3	3.3	7
	mbbopt	–	Ball–Berry model equation slope	4	12	8

Note. The ranges are based on (1) observations at the UIUC Energy Farm for 2008 for \bar{T}_p and from 2009 to 2018 for \bar{T}_s , (2) expert judgment (in the case where there is insufficient literature, but within 50% would be inappropriate), (3) Li, Yue, et al. (2018), (4) Cheng et al. (2020), (5) Dietzel et al. (2017), (6) Ma and Dwyer (2001), (7) Ricciuto et al. (2018), and (8) Personal communication with Dr. Dan Ricciuto.

spin-up mode, followed by a transient run from 1850 to 2008. For the transient run meteorological forcing data collected at the site was used for model simulation (Section 3.3). The model output was postprocessed by estimating daily average over the last 10 years of the transient run for the four output QoIs—gross primary productivity (GPP), ecosystem respiration (ER), latent heat flux (LE), and sensible heat flux (H). The estimated daily average for all ensemble members was then used for developing surrogates for each day of the year and for all four QoIs. We employed polynomial chaos surrogate form for developing surrogates as it provides flexible representation of the inputs and outputs as random variables (Ghanem & Spanos, 1991), and, at the same time, allows for exact analytical extraction of global sensitivity indices via variance decomposition (Crestaux et al., 2009). We utilized 1,600 of the 2,000 ELM simulations for developing the polynomial chaos surrogates and 400 simulations for testing the accuracy of the surrogates. In our case, where the inputs are randomly and uniformly sampled over their respective ranges, the surrogate construction reduces to a polynomial regression (Sargsyan, 2017). Finally, due to large number of input parameters, we employed Bayesian compressive sensing algorithm (Ricciuto et al., 2018; Sargsyan et al., 2014) to regularize the regression, arriving at a sparse polynomial set with only the relevant polynomial chaos bases activated. The surrogate construction, the associated GSA as well as the surrogate-enabled model calibration are carried out using the UQ Toolkit (Debusschere et al., 2016).

3.2. Global Sensitivity Analysis

Sobol sensitivity indices were used to examine the impact of parametric uncertainty on model outputs (Saltelli et al., 2010; Sobol, 2001). These indices provide an estimate of the fraction of variance contributed by each parameter or group of parameters toward the total variance in the output variable (Ricciuto et al., 2018). A major convenience of using PC polynomial chaos surrogates is that one can extract the sensitivity indices with

Table 2
Calibration and Validation Years for Miscanthus and Switchgrass

Crop	Calibration years	Validation years
Miscanthus	2009–2013, 2016, 2017, and 2018	2014 and 2015
Switchgrass	2009–2013	2014 and 2015

analytically available formulae without any additional sampling (Crestaux et al., 2009). In this study, we evaluate the main effect sensitivity that examines the contribution of one parameter at a time on the total variance (Figure 2).

3.3. Site Data

The observational data utilized for model calibration and validation was collected at the University of Illinois Urbana-Champaign (UIUC) Energy Farm located in the Midwest region of the United States. The mean annual precipitation at the UIUC Energy Farm is 1,009 mm and the mean annual temperature is 10.9°C with large seasonal variation ranging from monthly minimum below -5°C in winter to monthly maximum above 25°C in summer (Moore et al., 2021). The soil at the UIUC Energy Farm is deep and poorly drained silty clay loam. Both miscanthus (US-UiB) and switchgrass (US-UiA) plots were planted in the spring of 2008, however supplementary miscanthus was planted in 2009 and 2010 due to poor establishment in 2008 (Anderson-Teixeira et al., 2013). Nitrogen fertilizer was applied every year to switchgrass and from 2014 to 2018 to miscanthus at the rate of $56 \text{ kg ha}^{-1} \text{ yr}^{-1}$. Switchgrass was harvested at the end of the growing season in November or December, while miscanthus was harvested in the winter months of February or March. Eddy covariance flux towers at the center of the plots measure carbon, water, and energy fluxes at 30-min intervals, along with common meteorological variables (Moore et al., 2020; Zeri et al., 2011). Meteorological forcing data collected at the site including, air temperature, precipitation, downward shortwave radiation, downward longwave radiation, humidity, air pressure, and wind speed, was utilized for model simulation. GPP and ER were calculated from flux tower net ecosystem exchange values as per Moore et al. (2020). The flux tower derived GPP and ER are referred to as observed GPP and ER, respectively, in the remainder of the manuscript. GPP, ER, LE, and H values were available from 2009 to 2018 for miscanthus and from 2009 to 2015 for switchgrass. LAI was measured weekly during the peak growing season from 2014 to 2018 for miscanthus and from 2014 to 2015 for switchgrass, while harvest was measured annually for all growing years. Two years of measured carbon flux, energy flux, LAI, and crop yield data were used for validating the model. Carbon and energy flux measurements from the other years were used for model calibration (Table 2).

3.4. Bayesian Calibration via Markov Chain Monte Carlo

Bayesian inference was utilized for calibrating model parameters to improve the model performance with respect to site data (Tarantola, 2005). Specifically, we employ Markov chain Monte Carlo which samples input parameter space with an acceptance/rejection mechanism relying on the match of the model with the observational data encapsulated by a likelihood function. However, Markov chain Monte Carlo typically requires infeasibly large number of model evaluations before it arrives to a representative set of parameter samples. For this reason, we employ the pre-constructed, computationally inexpensive surrogate models in the Markov chain Monte Carlo loop. Calibration was performed simultaneously for all four QoIs to identify a single set of parameter value for each crop. Calibration was performed by utilizing carbon and energy flux measurements for the calibration years only (Table 2). A calibration window was first identified for both perennial bioenergy crops since all four QoIs had low or negligible values during the non-growth period. We tested four different calibration windows for GPP that excluded the winter months with minimal crop growth (Table S1 in Supporting Information S1). We found that a calibration window of 60–270 for both miscanthus and switchgrass resulted in both low root mean squared error (RMSE) and percent bias between observations and mean of the posterior simulations. For both miscanthus and switchgrass, the same calibration window was used for all four QoIs.

3.5. Model Validation

The optimized parameters obtained from model calibration were utilized for running a single model simulation for each crop. Similar to the calibration runs, the validation simulation ran for 200 years in the accelerated spin-up mode, 200 years in the non-accelerated spin-up mode, followed by a transient run from 1850 to 2015. For performing model validation, we compared simulated carbon fluxes, energy fluxes, LAI, and annual crop yield to the observations for the validation years (Table 2).

4. Results

4.1. Ensemble Evaluation

The ensemble captures observed seasonality and peak GPP values for both perennial bioenergy crops (Figures 1a and 1b). The seasonality of the perennial bioenergy crops, marked by the start and end of the growing season, is around 50 days longer than that of traditional maize grown in the midwestern USA (Cheng et al., 2020). The modified ELM model captures this longer growing season. Leaf onset for both perennial bioenergy cropping systems starts at approximately the same time but switchgrass GPP increases and declines earlier than miscanthus. The resulting slightly shifted growing seasons for the two perennial bioenergy crops was well captured by the ELM ensemble runs. Similar to seasonality, the model closely captures GPP values during the peak growing season, including the large observed interannual variability (light gray lines in Figures 1a and 1b).

The model simulates ecosystem respiration well for both crops, during both growth and non-growth periods (Figures 1c and 1d). During the growing season, the ensemble captures the full range of ER values. However, during the non-growth period the low observed ER values were simulated only by a small fraction of the ensemble members with the majority of ensemble members over predicting the ER during this period. The model simulated large negative spikes in late fall, is a caveat of the crop model eliminating excess maintenance respiration pool at harvest time (Oleson et al., 2013). This excess maintenance respiration pool is maintained by the model to supply carbon to plants during periods of low photosynthesis but is not required after harvest.

The ensemble captures the seasonality and observed extent of the energy fluxes during the growth phase (Figures 1e–1h). Similar to ER, the full range of LE during the growing season was captured by the ensemble. However, during the non-growth period the model ensemble underestimates the interannual variability in LE. The seasonal dynamics of H was not fully captured by the ensemble with the majority of ensemble members overpredicting H during the growing season. The observed trough of H during the growing season maybe be caused by increased amount of moisture available for evapotranspiration during the summer months that reduces the sensible heat fraction of net energy. The increased moisture availability was likely not captured in the meteorological forcing used for model simulation resulting in modeled H being higher than observations. During the non-growth period, the ensemble simulation for H underestimates both the observed mean and the large interannual variability.

4.2. ELM Surrogate Performance

The ELM surrogates provided fairly accurate representation of ELM simulations. We utilized 1,600 of the 2,000 ELM simulations for training the surrogates and 400 simulations for testing the accuracy of the surrogates. The testing data points were close to center diagonal line, representing agreement between surrogate and ELM simulations (green dots in Figures S1 and S2 in Supporting Information S1). The daily RMSE and relative RMSE between surrogate and ELM simulations for testing data points was relatively low during the growing season for all four QoIs for both perennial bioenergy crops, with few outliers during the non-growth period (Figures S3 and S4 in Supporting Information S1). These outliers during non-growth season however, did not impact the results of calibration as they fell outside of the calibration window and were therefore not utilized for GSA and calibration (Section 3.4). The average daily RMSE for miscanthus was 0.65 ($\text{gC m}^{-2} \text{day}^{-1}$) for GPP, 0.53 ($\text{gC m}^{-2} \text{day}^{-1}$) for ER, 3.66 (W m^{-2}) for LE, and 3.05 (W m^{-2}) for H while the relative RMSE for the same QoIs was 0.15, 0.14, 0.93, and 0.64, respectively. For switchgrass the average daily RMSE was 0.71 for GPP, 0.58 for ER, 3.95 for LE, and 2.78 for H while the relative RMSE for the same QoIs was 0.19, 0.16, 1.56, and 0.73, respectively.

4.3. Parameter Sensitivity

The most sensitive parameters for GPP, LE, and H vary with phenological state (Figures 1a, 2b and 2e–2h) while for ER they remain the same throughout the year, although their relative sensitivity changes with phenological stage (Figures 2c and 2d). For both perennial bioenergy crops, the parameter associated with stomatal conductance (`mbopt`) was the most sensitive parameter for all four QoIs while the parameter associated with leaf CN allocation (`leafcn`) was influential for GPP and ER. This parameters was most influential for GPP only during the growth phase but for ER, LE, and H it remains sensitive for most of the year. The parameter controlling leaf senescence (`senescence_temp`) was one of the most influential parameters during the leaf senescence period

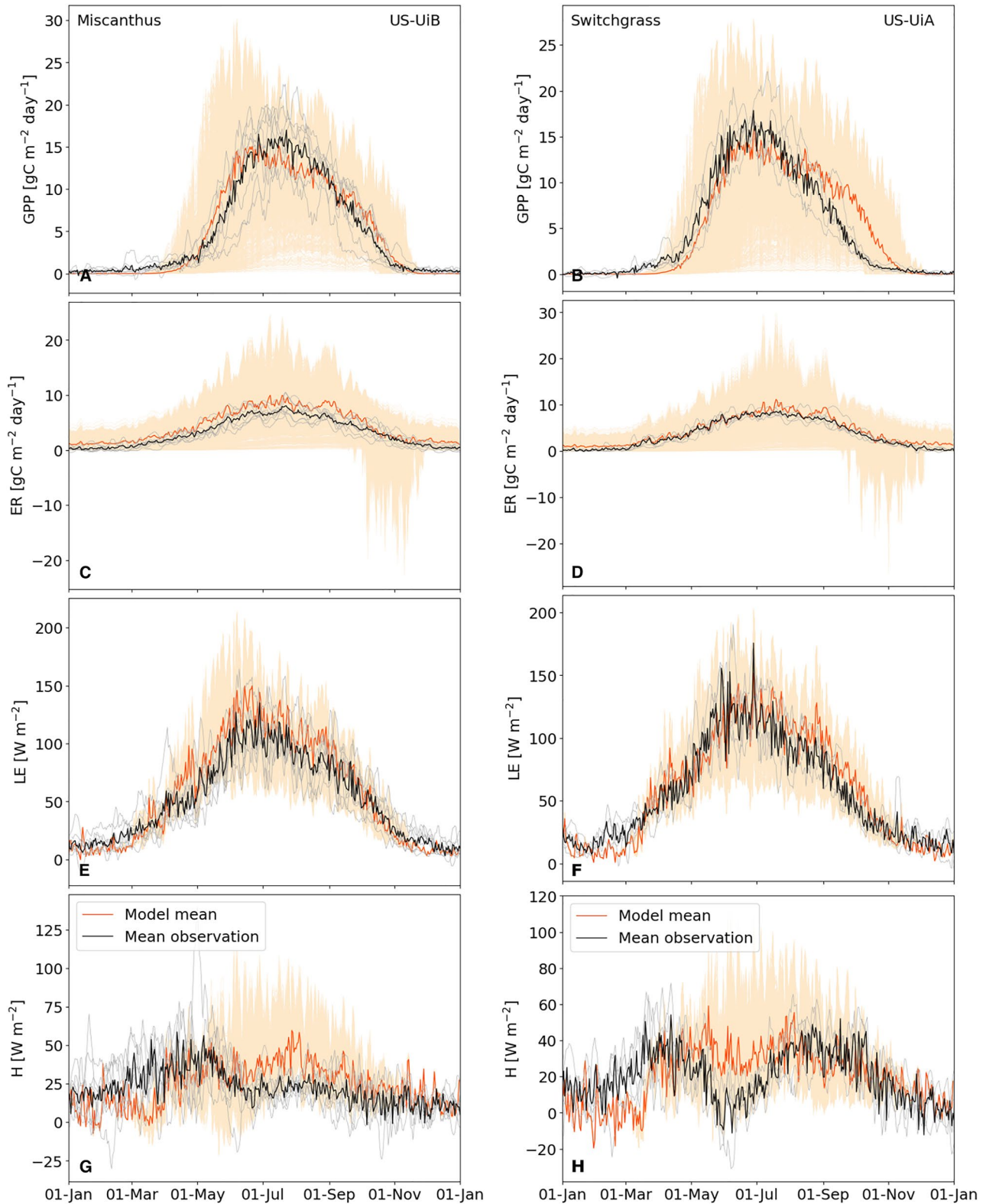


Figure 1. Simulated (light orange lines) and observed (gray lines) daily gross primary productivity (GPP) ($\text{gC m}^{-2} \text{day}^{-1}$) (a and b), ecosystem respiration (ER) ($\text{gC m}^{-2} \text{day}^{-1}$) (c and d), latent heat flux (LE) (W m^{-2}) (e and f) and, sensible heat flux (H) (W m^{-2}) (g and h) for miscanthus and switchgrass (left and right column, respectively). Light orange lines represent the simulated values for the 2,000 ensemble members. Gray lines represent daily observed values for the calibration years (Table 2). The thick orange line represents the simulated mean while the thick black line is the observed daily average across the calibration years. The observational data was collected at the University of Illinois Energy Farm.

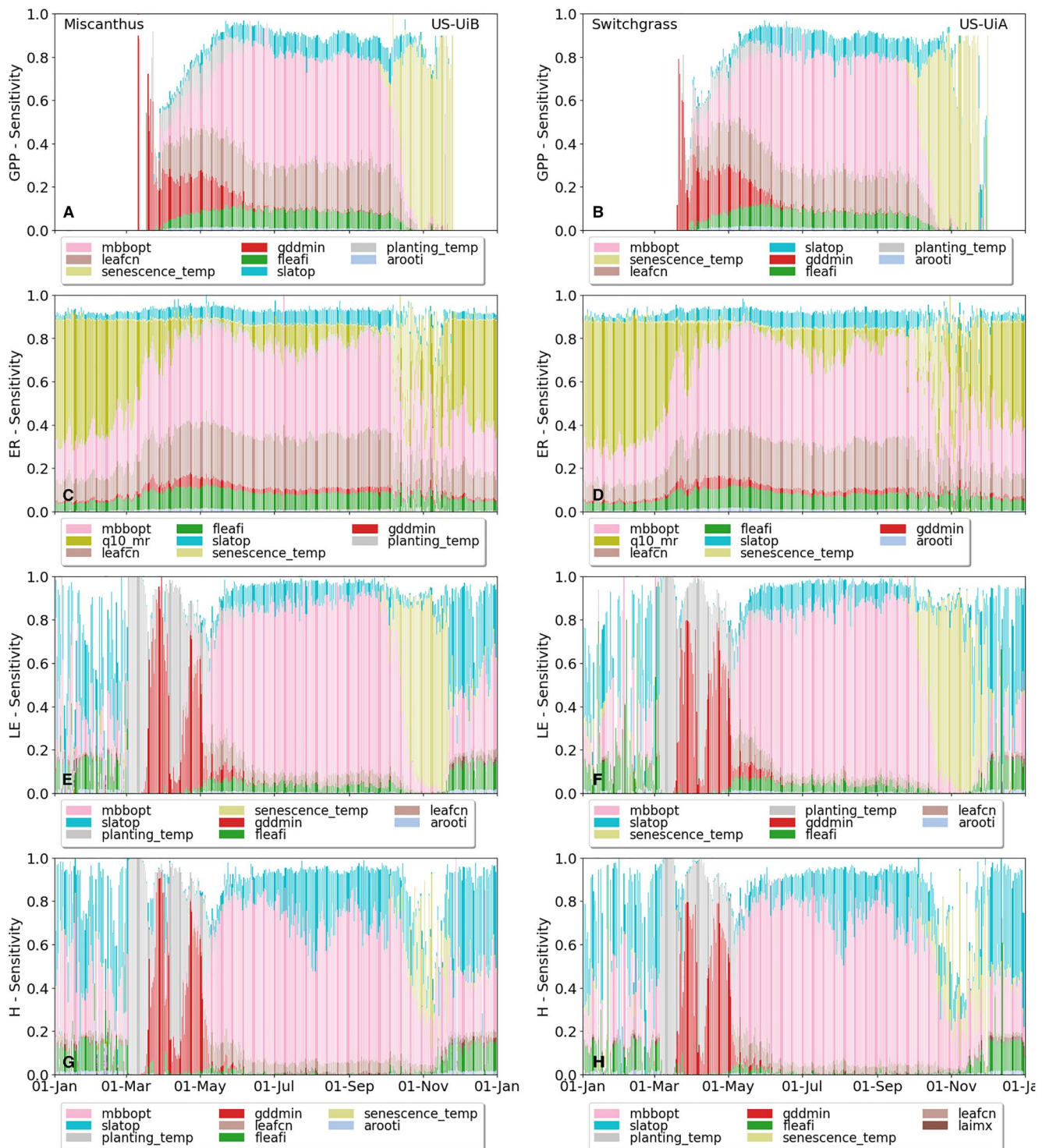


Figure 2. Main-effect Sobol sensitivity indices of the 20 parameters for the daily gross primary productivity (GPP) (a and b), ecosystem respiration (ER) (c and d), latent heat flux (LE) (e and f) and, sensible heat flux (H) (g and h) outputs for miscanthus and switchgrass (left and right column, respectively). The legend lists only the most influential parameters for the respective quantities of interests.

for GPP, ER, and LE. During the non-growth period, the temperature sensitivity for maintenance respiration (q_{10_mr}) parameter was the most sensitive parameter for ER. For GPP, LE, and H , during the leaf emergence phase, the parameter controlling leaf onset ($gddmin$) exhibits high sensitivity. For LE and H , $planting_temp$ also exhibited high sensitivity during leaf emergence phase. The five most influential parameters across the four

Table 3
Optimized Parameter Values for Five Most Sensitive Parameters Based on Maximum a Posteriori (MAP) Estimates

Parameter	ELM variable	Description	Input range	Miscanthus	Switchgrass
\overline{GDD}^{\min}	gddmin	Minimum growing degree days	50–320	136	51 ^a
\overline{T}_s	senescence_temp	Average 10-day temperature for leaf senescence	280–290	290 ^a	290 ^a
	leafcn	Leaf CN ratio	15–35	35 ^a	34
	q10_mr	Temperature sensitivity for MR	1.3–3.3	2.1	2.2
	mbbopt	Ball–Berry model equation slope	4–12	8.1	8.3

^aThe probability density function of the optimized parameter range was skewed to either side of the input range.

QoIs, mbbopt, leafcn, senescence_temp, q10_mr, and gddmin, were used for conducting a combined calibration with all QoIs.

4.4. Model Calibration

The optimized parameter values for select parameters were mostly similar across the two bioenergy crops (Table 3). These values represent the maximum a posteriori estimates of the optimized parameter range obtained after conducting calibration for the five most sensitive parameters (Figure S5 in Supporting Information S1). A reliable range for optimal senescence_temp for both crops was not obtained since senescence_temp was only sensitive during the last few months of the year that falls outside the calibration window. Additionally, the optimized value of leafcn for miscanthus and gddmin for switchgrass are less reliable as the probability density function (pdf) of the optimized parameter are skewed toward either side of the input range (Figure S5 in Supporting Information S1), indicating a degree of overfitting or a need to increase the parameter range. The non-optimum values for these parameters may result in possible bias between simulated and observed fluxes or slight shifts in the start of the leaf onset compared to the observations (controlled by gddmin). Such less reliable estimate of few parameters is not unexpected since various land process are interlinked, and some parameters may not have been included in our GSA resulting in overfitting of other parameters. Despite this limitation, the approach utilized here identifies the most influential parameters and the optimum value of several of these parameters. Default parameter values were used for parameters that were not optimized as part of the GSA.

The calibrated GPP closely matches the observations for the timing of leaf onset, timing of peak GPP, the sharp increase before peak GPP, and the timing of leaf senescence for both perennial bioenergy crops, but slightly underestimates the magnitude of peak GPP (Figures 3a and 3b black line and green shading). Overall, the posterior GPP estimates explained more than 90% of the observed daily variance within the calibration window and for all year round for both miscanthus and switchgrass (Table 4). The percent bias for miscanthus was less than 12% and for switchgrass was less than 6% within the calibration window.

The calibrated ER closely matches the observations during the growing period and was slightly higher than the observations during the non-growing season for both crops (Figures 3b and 3d). Similar to GPP, the posterior ER estimates explain large fraction of the observed daily variance (more than 95%). The higher observed percent bias during the calibration window for both perennial bioenergy crops, despite closely matching the observations, can most likely be attributed to the daily variations.

The posterior estimates of latent heat flux captures the observed seasonality and peak magnitude for both crops during the growing season, however calibrated sensible heat flux captures only the observed seasonality for switchgrass (Figures 3e–3h). The calibrated latent heat flux explains more than 85% of the observed daily variation while the sensible heat flux explains 2%–43% (Table 4). The higher/lower explanatory power of LE/H for observed daily variation is likely due to increased amount of moisture available during summer for evapotranspiration that results in LE dominating the energy balance. Similar to ER, the large percent bias for LE despite closely matching the observations is likely due to difference in values at a daily timescale. Although, the posterior H estimates for switchgrass, capture the seasonality in the observations they fail to capture the observed magnitude during the months of May–July. The posterior estimates capture the observed increase in switchgrass

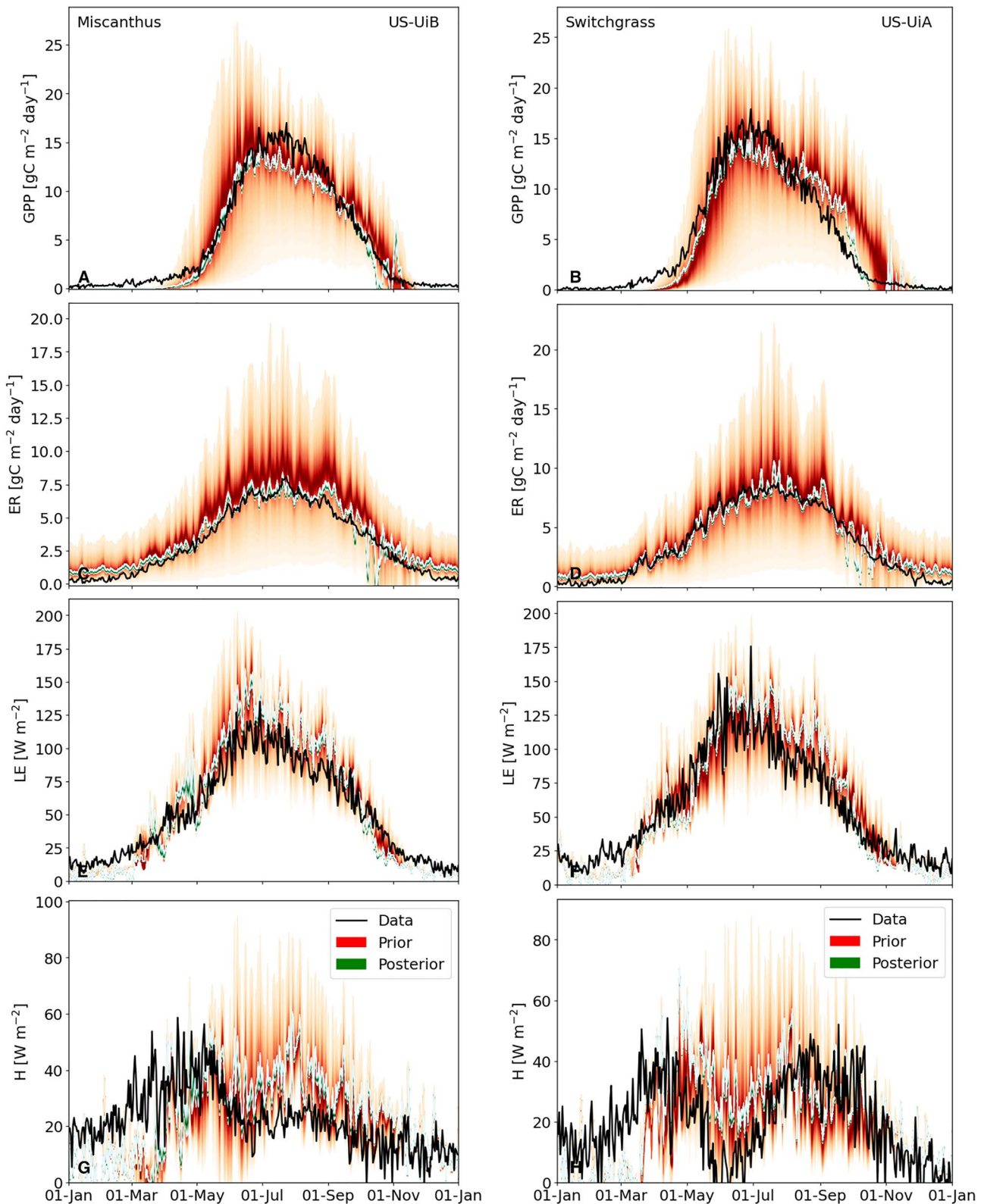


Figure 3. Model calibration: observed versus prior and posterior distribution of the modeled gross primary productivity (GPP) ($\text{gC m}^{-2} \text{day}^{-1}$) (a and b), ecosystem respiration (ER) ($\text{gC m}^{-2} \text{day}^{-1}$) (c and d), latent heat flux (LE) (W m^{-2}) (e and f) and, sensible heat flux (H) (W m^{-2}) (g and h) for miscanthus and switchgrass (left and right column, respectively). The prior distribution (red shade) represents the daily simulated values for the 2,000 ensemble members while the posterior distribution (green shade) represents the calibrated values estimated with the optimized parameters. A calibration window from 60 to 270 days was utilized for both miscanthus and switchgrass. The black line represents observed average daily across the calibration years (Table 2).

Table 4

Root Mean Squared Error (RMSE), Percent Bias, Correlation Coefficient, and R^2 Between Observations and Mean of Surrogate Based Posterior Simulations

	Miscanthus within calibration window (60–270)				Switchgrass within calibration window (60–270)			
	GPP	ER	LE	H	GPP	ER	LE	H
RMSE	1.58	0.63	20.43	17.16	1.91	0.72	21.48	18.27
Percent bias (%)	−11.59	7.67	16.91	17.07	−5.55	−0.65	7.83	19.77
Corr. coeff.	0.99	0.98	0.96	0.14	0.97	0.98	0.92	0.41
R^2	0.98	0.97	0.91	0.02	0.94	0.96	0.85	0.17
	Miscanthus considering all 365 days				Switchgrass considering all 365 days			
	GPP	ER	LE	H	GPP	ER	LE	H
RMSE	1.41	0.77	17.11	15.81	2.05	0.84	18.28	16.19
Percent bias (%)	−13.9	13.08	7.03	9.37	−10.54	6.06	0.03	7.99
Corr. coeff.	0.99	0.98	0.98	0.55	0.97	0.98	0.97	0.66
R^2	0.98	0.96	0.96	0.3	0.94	0.96	0.94	0.43

Note. All listed R^2 are significant with $p < 0.01$.

H between August and September (Figure 3h). However, this increase in late summer H was not observed in miscanthus (black line Figure 3g) implying different agricultural management between the two crops during this period that was not represented in the model resulting in posterior estimates for miscanthus being higher than observations. It is also noteworthy that the observed daily average used for calibration has a higher signal-to-noise ratio for both the energy fluxes than for the carbon fluxes, likely contributing to lower calibration accuracy for the energy fluxes.

4.5. Model Validation

We found that the calibrated model generally captures the observed seasonality of the carbon and energy fluxes and simulated flux magnitude (Figure 4). The seasonality of switchgrass was better simulated than that of miscanthus, for which the simulated leaf emergence starts earlier than observations. For both crops, simulated flux magnitudes in the earlier and later part of the growing season closely match the observations, although the peak fluxes were not as well captured. The model underestimates peak GPP for both crops, peak ER for switchgrass, and overestimates the peak ER and LE for miscanthus. The simulated sensible heat flux for miscanthus fails to capture the observed seasonality and magnitude of observations. These differences maybe due to one or more of these factors: all four QoIs were calibrated simultaneously, yielding optimum value across the four QoIs but not for individual QoIs; the combined calibration step limited the number of parameters that were selected for calibration; and observations for the validation years were different than those used for calibration, that is, the model did not perform as well for 'unseen' years.

We found that simulated LAI captured the observed seasonality, but underestimated the magnitude (Figure 5). LAI was estimated in the model as the product of leaf carbon and a parameter specifying leaf area at the top of the canopy ($slatop$). The $slatop$ parameter was considered in our GSA study but was not among the five most influential parameters across the four QoIs and thus its default value (0.05) was used. The low simulated LAI for switchgrass compared to the observations suggest a higher $slatop$ value than the current model default.

Interestingly, the model underestimates annual harvest for both crops with larger difference between observations and simulated values for miscanthus than switchgrass (Figure 6). The disparity between observed and simulated yield is likely due to simulated LAI being lower than observed (Figure 5) and due to harvest occurring earlier in the model (the later part of October) than at the UIUC Energy Farm (between January and March of the following year for miscanthus, and between November and December for switchgrass) (Anderson-Teixeira et al., 2013). The larger difference between observed and modeled harvest dates for miscanthus compared to switchgrass translates into larger discrepancy in observed and modeled harvest amounts for miscanthus compared to switchgrass. It is also noteworthy, that for miscanthus yield peaks a few years after crop establishment and both validation years occur after the crop is well established resulting in the observed yield for these years toward the higher end of

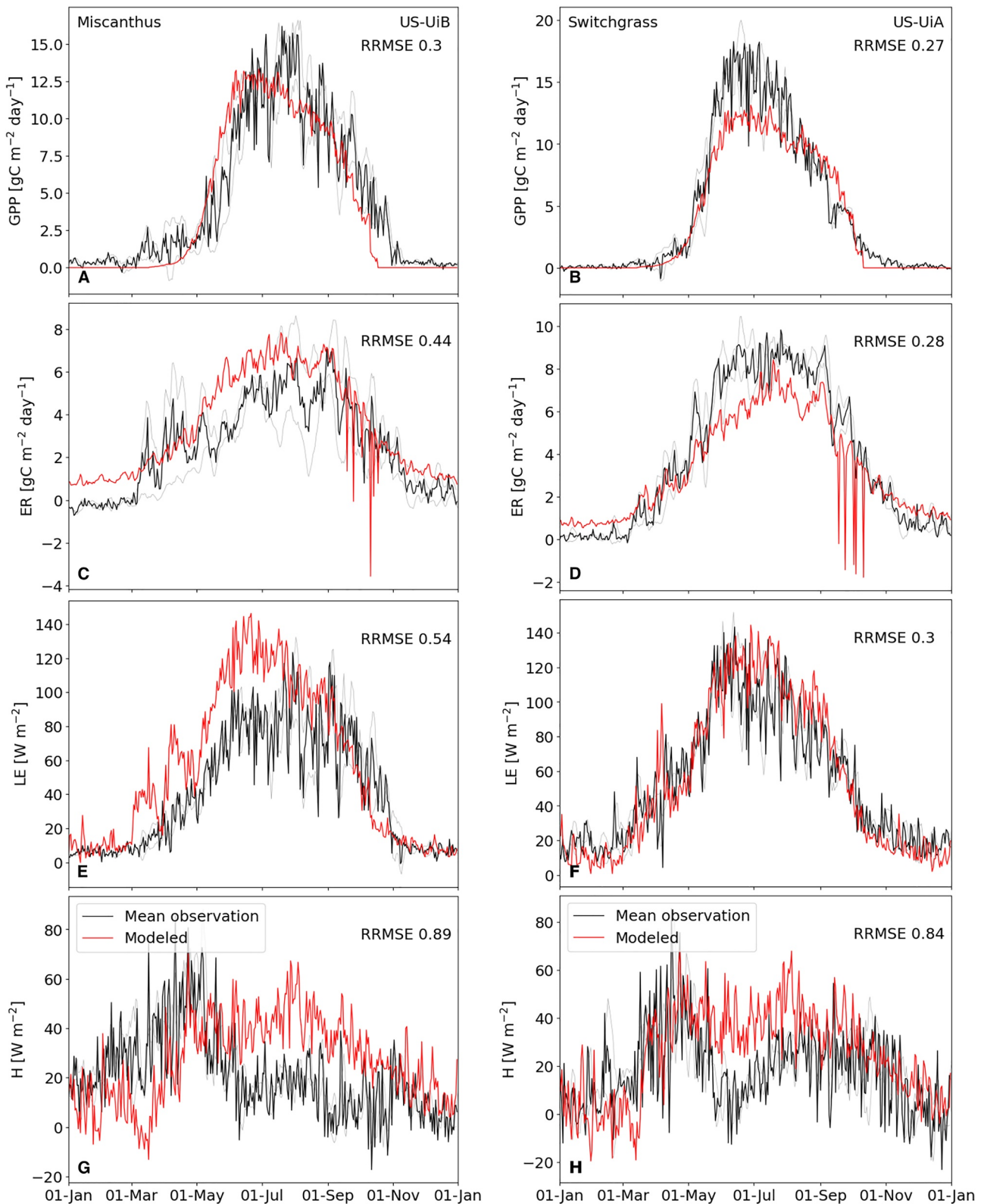


Figure 4. Model validation: observed versus simulated gross primary productivity (GPP) ($\text{gC m}^{-2} \text{day}^{-1}$) (a and b), ecosystem respiration (ER) ($\text{gC m}^{-2} \text{day}^{-1}$) (c and d), latent heat flux (LE) (W m^{-2}) (e and f) and, sensible heat flux (H) (W m^{-2}) (g and h) for miscanthus and switchgrass (left and right column, respectively) using optimized parameter values (Table 3). The red lines represent daily average model simulation over the last 10 years of transient run and the black line represents observed daily average values over the validation years (Table 2).

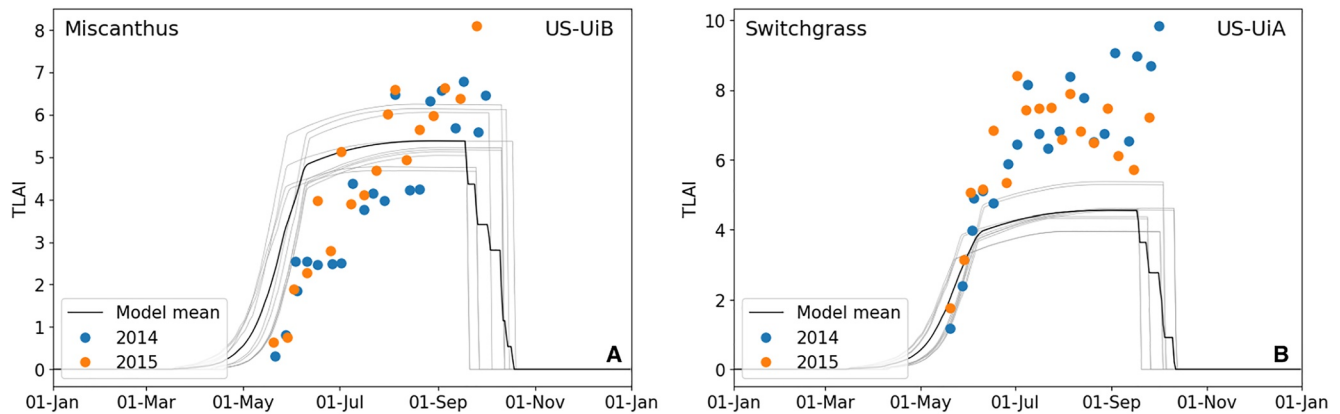


Figure 5. Model validation: observed versus simulated leaf area index (LAI) for miscanthus (a) and switchgrass (b) using optimized parameter value (Table 3). The gray lines represent simulated annual LAI over the last 10 years of transient run and the black line is the model mean across the 10 years. The dots represents observed weekly LAI over the validation years (Table 2).

the observed range across all years (mean yield across all years—13.2 ton ha⁻¹; mean yield over the validation years—15.7 ton ha⁻¹).

The fertilizer application rate of 56 kg ha⁻¹ yr⁻¹, at the UIUC Energy Farm, is lower than the ELM default of 84 kg ha⁻¹ yr⁻¹. We performed a sensitivity analysis to examine the impact of lower fertilizer application rate and found that lower fertilizer rate resulted in minimal changes to the carbon and energy fluxes estimation suggesting that the calibrated QoIs aren't sensitive to the fertilizer application rate.

5. Discussion

Only a handful of parameters dominate the sensitivity of carbon and energy fluxes for the two perennial bioenergy crops. The ELM crop model utilizes a large number of parameters each with its own uncertainty that results in a large spread in the simulated fluxes. The sensitivity analysis performed in this study shows that five out of more than 100 parameters used for the ELM crop model, dictate the uncertainty in modeled carbon and energy fluxes. This finding can assist in streamlining future model calibration efforts. Similar findings were also made for ELM simulated carbon cycle outputs from multiple plant functional types (Ricciuto et al., 2018). We find that for both carbon and energy fluxes parameters controlling the timing of leaf senescence (*senescence_temp*), onset of leaves (*gddmin*), and stomatal conductance (*mbbopt*) were among the most sensitive parameters. Additionally, for GPP and ER the parameter controlling leaf CN allocation (*leafcn*) and for ER the parameter controlling maintenance respiration (*q10_mr*) were also highly sensitive.

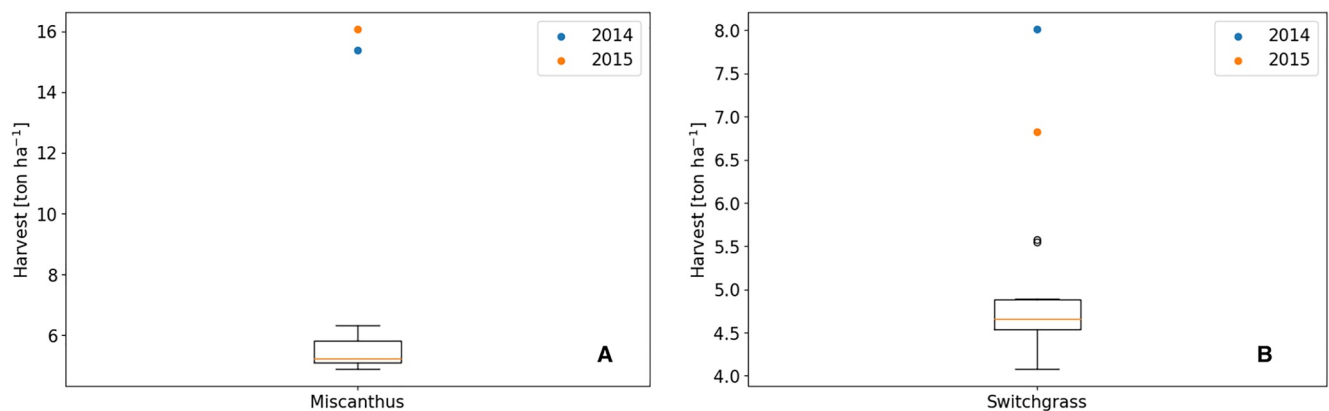


Figure 6. Model validation: observed versus simulated crop harvest for miscanthus (a) and switchgrass (b) using optimized parameter value (Table 3). The box plot represents distribution of simulated annual harvest over the last 10 years of transient run and the dots represents observed harvest for the validation years (Table 2).

Some of the most influential parameters identified in this study had not been previously identified. The parameters associated with phenology (`gddmin`, `senescence_temp`), stomatal conductance (`mbbopt`), and maintenance respiration (`q10_mr`) had not been identified before as influential for modeling carbon and energy fluxes for perennial crops. Another study modeling miscanthus and switchgrass using CLM5, identified `slatop`, `fleafi`, and parameters associated with photosynthetic capacity (`s_vc` and `i_vc`) as sensitive parameters for GPP, ER, and LE (Cheng et al., 2020). The `s_vc` and `i_vc` parameters were considered in our analysis but were not found to be sensitive for carbon or energy fluxes, while the `slatop` and `fleafi` were influential parameters for select QoIs in this study but were not among the five most sensitive parameters combinedly across the four QoIs.

These differences are likely due to one or more of three major differences in these two studies. First, ELM and CLM5 both have several differences between them despite branching from the same model (CLM4.5). For instance, ELM now incorporates dynamic root modeling (Drewniak, 2019), climate driven planting date estimation, and perennial crop modeling while CLM5 includes the implementation of Fixation and Uptake of Nitrogen (FUN) and Leaf Use of Nitrogen for Assimilation (LUNA). The FUN model accounts for the carbon cost of nitrogen acquisition (Shi et al., 2016) while the LUNA model accounts for leaf nitrogen utilization in its photosynthetic capacity estimation (Ali et al., 2016). Second, both miscanthus and switchgrass were modeled as annual crops by Cheng et al. (2020) with four distinct phenological phases that include planting, leaf emergence, grain fill, and harvest, while in this study they are modeled as perennial crops that have only three phenological phases of crop emergence, leaf onset, and leaf senescence. The requirements for the start of various phenological phases also differ between this study and Cheng et al. (2020) and allows to accurately capture the timing of crop emergence, leaf onset, leaf senescence, and the growing season length of the two perennial bioenergy crops that are quite distinct from annual crops. Third, Cheng et al. (2020) conducted sensitivity analysis by varying 10 samples at equal increments within the input range, one parameter at a time. This approach ignores the effect of parameter interactions. The GSA approach utilized in this study accounts for parameter interactions by randomly varying all parameters within their input range to generate 2,000 parameter samples for running ELM. Additionally, ELM surrogates were developed from the outputs of 2,000 ELM runs that were then employed for surrogate based GSA. Due to these differences across the two studies, the optimized parameter values obtained in this study were compared to the literature rather than among themselves.

The calibrated value of `q10_mr` is comparable to observations. Studies examining the impact of temperature sensitivity on soil respiration found `q10_mr` to range between 1.6 and 3.2 with an average of 3.0 for miscanthus (Robertson et al., 2017; Yazaki et al., 2004) and to range between 2.3 and 3.8 with an average of 2.7 for switchgrass (Lee et al., 2007; Skinner & Adler, 2010). Variability across the year was also observed in `q10_mr` with highest values being observed during the growth period and lowest values during winter months (Robertson et al., 2017). The `q10_mr` range estimated in this study (Table 3) is close to observations but stays constant throughout the year in ELM. Interestingly, a study calibrating CLM4.5 for coniferous forest found that increasing `q10_mr` from ELM default of 1.5–2.5 better captured the observed seasonality of ER for needleleaf evergreen temperate forest (Duarte et al., 2017).

As expected, model simulated QoIs that were used for model calibration (GPP, ER, LE, and *H*) better captured the observed seasonality and magnitude for the validation years than QoIs that were not used for calibration (LAI and harvest). Simulated LAI, though not used for calibration, captured the observed seasonality for both crops, however, underestimated LAI magnitude. LAI estimation utilizes specific leaf area parameter (`slatop`) that has been observed to vary with the growing season, light availability, and photoperiod (Dohleman et al., 2009; Tian et al., 2015; Trócsányi et al., 2009; Van Esbroeck et al., 2003). Currently `slatop` in ELM does not vary with the growing season, light availability, or photoperiod and this lack of variation could be contributing to low estimated LAI. In addition, as noted above, `slatop` parameter was not optimized, and doing so might improve simulated LAI. Simulated harvest was lower than the observations likely due to harvest occurring earlier in the model than in the observations. Similar to our observations, studies comparing simulated yields against a global data set of observed yields (Li, Ciais, et al., 2018) have found modeled yields to be much higher or lower than observations at select locations (Li, Yue, et al., 2018; Littleton et al., 2020).

Interestingly, the optimized parameter values for the two bioenergy crops were quite close to each other. Studies have shown photosynthetic rates and productivity to differ significantly between miscanthus and switchgrass (Dohleman et al., 2009; Kiniry et al., 2012). Despite these differences among the two bioenergy crops, the similar

parameters values estimated in this study may be due to ELM likely being highly sensitivity to the most influential parameters identified in our study. It is also worth noting, that accurately capturing differences across pfts is challenging for ESMs in general, and is a subject of active research (Anderegg et al., 2022; Fisher et al., 2018).

The ELM-crop model has limitations that contribute to uncertainty in our predictions of carbon and energy fluxes. First, the model currently underpredicts harvest for perennial bioenergy crops, likely due to inaccuracies in the simulated harvest date. Additionally, underestimation of yield may also be due to improved agricultural management practices at the UIUC Energy farm that are not captured in ELM. This limitation should be further explored by future studies examining the impact of perennial bioenergy crop expansion. Second, parameters like `slatop` have been observed to vary with time and light availability, processes that are not captured by the time-invariant parameters currently used in the model. Third, parameters associated with maintenance respiration (`br_mr` and `q10_mr`) are currently held constant for all crop and vegetation types. However, as shown in this study and (Duarte et al., 2017) these parameters vary with plant and crop functional types. Fourth, agricultural management practices, such as fertilizer application rates, currently do not vary over time. The large increase in fertilizer application over the last few decades and the projected future changes should be captured in the model to accurately capture historical and future fluxes.

6. Conclusions

This study implements perennial crop modeling in ELM and calibrates and tests the model for miscanthus and switchgrass using observational data on carbon and energy fluxes from the Midwest United States. We find that only five parameters associated with leaf carbon nitrogen, timing of leaf onset and senescence, leaf stomatal conductance, and maintenance respiration, control the uncertainty in modeled carbon and energy fluxes. The calibrated model generally captures the observed seasonality of carbon and energy fluxes; some poorly simulated outputs (in particular sensible heat flux and harvest amount) could be due either to lack of accurate process representation, relevant parameters not being considered, or a large signal-to-noise ratio in the observations. Future studies can also include model outputs related to water budget in model calibration and validate the model using observations from other site. Our modeling study lays the groundwork for future studies that examine the impact of perennial bioenergy crop expansion and provides valuable insights for improving representation of other crops in ESMs. Future research can utilize the parameterized perennial bioenergy crop model developed in this study to examine the impact of future perennial bioenergy expansion on carbon, water, and energy budgets. Finally, future crop modeling studies that perform GSA can utilize only the most sensitive parameters identified in this study to reduce the surrogate models' dimensionality, and improve their accuracy.

Acknowledgments

This research was supported as part of the Energy Exascale Earth System Model (E3SM) project, funded by the U.S. Department of Energy, Office of Science, Office of Biological and Environmental Research. The Pacific Northwest National Laboratory is operated by Battelle for the US Department of Energy under Contract DE-AC05-76RLO1830. Sandia National Laboratories is a multimission laboratory managed and operated by National Technology and Engineering Solutions of Sandia, LLC, a wholly owned subsidiary of Honeywell International Inc., for the U.S. Department of Energy's National Nuclear Security Administration under contract DE-NA0003525. Dr. Katherine Calvin is currently detailed to the National Aeronautics and Space Administration. Dr. Calvin's contributions to this article occurred prior to her detail. The views expressed are her own and do not necessarily represent the views of the National Aeronautics and Space Administration or the United States Government. We also thank anonymous reviewers for their thoughtful comments that helped to significantly improve the manuscript.

Data Availability Statement

The E3SM model is described in detail at <https://e3sm.org/>. The source code for E3SM v2 can be downloaded from <https://www.osti.gov/doecode/biblio/64702>. The source code for ELMv2 that contains perennial bioenergy crops is archived and made publicly available at <https://doi.org/10.5281/zenodo.5975834>. Model output data are accessible directly from the DOE's National Energy Research Scientific Computing Center (NERSC) at <https://portal.nersc.gov/cfs/e3sm/esinha/Sinha-et-al-2022-JAMES/>. All of the code supporting this paper is available at <https://github.com/evasinha/Sinha-et-al-2022-JAMES>. The UIUC Energy Farm data used in this study can be obtained from the AmeriFlux websites: US-UiA: <https://ameriflux.lbl.gov/sites/siteinfo/US-UiA> and US-UiB: <https://ameriflux.lbl.gov/sites/siteinfo/US-UiB>.

References

- Ali, A. A., Xu, C., Rogers, A., Fisher, R. A., Wullschlegler, S. D., Massoud, E., et al. (2016). A global scale mechanistic model of photosynthetic capacity (LUNA V1. 0). *Geoscientific Model Development*, 9(2), 587–606. <https://doi.org/10.5194/gmd-9-587-2016>
- Anderegg, L. D., Griffith, D. M., Cavender-Bares, J., Riley, W. J., Berry, J. A., Dawson, T. E., & Still, C. J. (2022). Representing plant diversity in land models: An evolutionary approach to make “functional types” more functional. *Global Change Biology*, 28(8), 2541–2554. <https://doi.org/10.1111/gcb.16040>
- Anderson-Teixeira, K. J., Masters, M. D., Black, C. K., Zeri, M., Hussain, M. Z., Bernacchi, C. J., & DeLucia, E. H. (2013). Altered belowground carbon cycling following land-use change to perennial bioenergy crops. *Ecosystems*, 16(3), 508–520. <https://doi.org/10.1007/s10021-012-9628-x>
- Boas, T., Bogenia, H., Grünwald, T., Heinesch, B., Ryu, D., Schmidt, M., et al. (2021). Improving the representation of cropland sites in the Community Land Model (CLM) version 5.0. *Geoscientific Model Development*, 14(1), 573–601. <https://doi.org/10.5194/gmd-14-573-2021>

- Burrows, S., Maltrud, M., Yang, X., Zhu, Q., Jeffery, N., Shi, X., et al. (2020). The DOE E3SM v1.1 biogeochemistry configuration: Description and simulated ecosystem-climate responses to historical changes in forcing. *Journal of Advances in Modeling Earth Systems*, 12(9), e2019MS001766. <https://doi.org/10.1029/2019MS001766>
- Cheng, Y., Huang, M., Chen, M., Guan, K., Bernacchi, C., Peng, B., & Tan, Z. (2020). Parameterizing perennial bioenergy crops in version 5 of the Community Land Model based on site-level observations in the Central Midwestern United States. *Journal of Advances in Modeling Earth Systems*, 12(1), e2019MS001719. <https://doi.org/10.1029/2019MS001719>
- Cheng, Y., Huang, M., Zhu, B., Bisht, G., Zhou, T., Liu, Y., et al. (2021). Validation of the Community Land Model version 5 over the Contiguous United States (CONUS) using in situ and remote sensing data sets. *Journal of Geophysical Research: Atmospheres*, 126(5), e2020JD033539. <https://doi.org/10.1029/2020JD033539>
- Crestaux, T., Le Maître, O., & Martinez, J. (2009). Polynomial chaos expansion for sensitivity analysis. *Reliability Engineering & System Safety*, 94(7), 1161–1172. <https://doi.org/10.1016/j.res.2008.10.008>
- Debusschere, B., Sargsyan, K., Safta, C., & Chowdhary, K. S. (2016). *UQTK: A C++/python toolkit for uncertainty quantification* (Tech. Rep.). Sandia National Lab. (SNL-CA).
- Dietzel, R., Liebman, M., & Archontoulis, S. (2017). A deeper look at the relationship between root carbon pools and the vertical distribution of the soil carbon pool. *Soils*, 3(3), 139–152. <https://doi.org/10.5194/soil-3-139-2017>
- Dohleman, F., Heaton, E., Leakey, A., & Long, S. (2009). Does greater leaf-level photosynthesis explain the larger solar energy conversion efficiency of *Miscanthus* relative to switchgrass? *Plant, Cell and Environment*, 32(11), 1525–1537. <https://doi.org/10.1111/j.1365-3040.2009.02017.x>
- Drewniak, B. (2019). Simulating dynamic roots in the Energy Exascale Earth System Land Model. *Journal of Advances in Modeling Earth Systems*, 11(1), 338–359. <https://doi.org/10.1029/2018MS001334>
- Drewniak, B., Song, J., Prell, J., Kotamarthi, V., & Jacob, R. (2013). Modeling agriculture in the Community Land Model. *Geoscientific Model Development*, 6(2), 495–515. <https://doi.org/10.5194/gmd-6-495-2013>
- Duarte, H. F., Raczka, B. M., Ricciuto, D. M., Lin, J. C., Koven, C. D., Thornton, P. E., et al. (2017). Evaluating the Community Land Model (CLM4.5) at a coniferous forest site in northwestern United States using flux and carbon-isotope measurements. *Biogeosciences*, 14(18), 4315–4340. <https://doi.org/10.5194/bg-14-4315-2017>
- FAO. (2021). *FAOSTAT. Food and Agriculture Organization of the United Nations* (Tech. Rep.). Author.
- Fargione, J., Hill, J., Tilman, D., Polasky, S., & Hawthorne, P. (2008). Land clearing and the biofuel carbon debt. *Science*, 319(5867), 1235–1238. <https://doi.org/10.1126/science.1152747>
- Fisher, R. A., Koven, C. D., Anderegg, W. R., Christoffersen, B. O., Dietze, M. C., Farrior, C. E., et al. (2018). Vegetation demographics in Earth system models: A review of progress and priorities. *Global Change Biology*, 24(1), 35–54. <https://doi.org/10.1111/gcb.13910>
- Georgescu, M., Lobell, D. B., & Field, C. B. (2011). Direct climate effects of perennial bioenergy crops in the United States. *Proceedings of the National Academy of Sciences*, 108(11), 4307–4312. <https://doi.org/10.1073/pnas.1008779108>
- Ghanem, R., & Spanos, P. (1991). *Stochastic finite elements: A spectral approach*. Springer Verlag.
- Golaz, J.-C., Caldwell, P. M., Van Roekel, L. P., Petersen, M. R., Tang, Q., Wolfe, J. D., et al. (2019). The DOE E3SM coupled model version 1: Overview and evaluation at standard resolution. *Journal of Advances in Modeling Earth Systems*, 11(7), 2089–2129. <https://doi.org/10.1029/2018MS001603>
- Golaz, J.-C., Van Roekel, L. P., Zheng, X., Roberts, A. F., Wolfe, J. D., Lin, W., et al. (2022). The DOE E3SM Model Version 2: Overview of the physical model and initial model evaluation. *Journal of Advances in Modeling Earth Systems*, 14(12), e2022MS003156. <https://doi.org/10.1029/2022ms003156>
- IPCC. (2018). *Global warming of 1.5°C: An IPCC special report on the impacts of global warming of 1.5°C above pre-industrial levels and related global greenhouse gas emission pathways, in the context of strengthening the global response to the threat of climate change, sustainable development, and efforts to eradicate poverty*. Intergovernmental Panel on Climate Change.
- Kiniry, J. R., Johnson, M.-V. V., Bruckerhoff, S. B., Kaiser, J. U., Cordsiemon, R., & Harmel, R. D. (2012). Clash of the titans: Comparing productivity via radiation use efficiency for two grass giants of the biofuel field. *BioEnergy Research*, 5(1), 41–48. <https://doi.org/10.1007/s12155-011-9116-8>
- Klein Goldewijk, K., Beusen, A., Doelman, J., & Stehfest, E. (2017). Anthropogenic land use estimates for the Holocene–HYDE 3.2. *Earth System Science Data*, 9(2), 927–953. <https://doi.org/10.17026/dans-25g-gez3>
- Lambert, F. H., Harris, G. R., Collins, M., Murphy, J. M., Sexton, D. M., & Booth, B. B. (2013). Interactions between perturbations to different Earth system components simulated by a fully-coupled climate model. *Climate Dynamics*, 41(11), 3055–3072. <https://doi.org/10.1007/s00382-012-1618-3>
- Langholtz, M. H., Stokes, B. J., & Eaton, L. M. (2016). 2016 Billion-ton report: Advancing domestic resources for a thriving bioeconomy, volume 1: Economic availability of feedstock. *Oak Ridge National Laboratory, Oak Ridge, Tennessee, managed by UT-Battelle, LLC for the US Department of Energy*, 2016, 1–411.
- Lee, D., Doolittle, J., & Owens, V. (2007). Soil carbon dioxide fluxes in established switchgrass land managed for biomass production. *Soil Biology and Biochemistry*, 39(1), 178–186. <https://doi.org/10.1016/j.soilbio.2006.07.004>
- Levis, S. (2010). Modeling vegetation and land use in models of the Earth system. *Wiley Interdisciplinary Reviews: Climate Change*, 1(6), 840–856. <https://doi.org/10.1002/wcc.83>
- Levis, S., Bonan, G. B., Kluzek, E., Thornton, P. E., Jones, A., Sacks, W. J., & Kucharik, C. J. (2012). Interactive crop management in the community Earth system model (CESM1): Seasonal influences on land–atmosphere fluxes. *Journal of Climate*, 25(14), 4839–4859. <https://doi.org/10.1175/JCLI-D-11-00446.1>
- Li, W., Ciais, P., Makowski, D., & Peng, S. (2018). A global yield dataset for major lignocellulosic bioenergy crops based on field measurements. *Scientific Data*, 5(1), 1–10. <https://doi.org/10.1038/sdata.2018.169>
- Li, W., Yue, C., Ciais, P., Chang, J., Goll, D., Zhu, D., et al. (2018). ORCHIDEE-MICT-BIOENERGY: An attempt to represent the production of lignocellulosic crops for bioenergy in a global vegetation model. *Geoscientific Model Development*, 11(6), 2249–2272. <https://doi.org/10.5194/gmd-11-2249-2018>
- Littleton, E. W., Harper, A. B., Vaughan, N. E., Oliver, R. J., Duran-Rojas, M. C., & Lenton, T. M. (2020). JULES-BE: Representation of bioenergy crops and harvesting in the Joint UK Land Environment Simulator vn5.1. *Geoscientific Model Development*, 13(3), 1123–1136. <https://doi.org/10.5194/gmd-13-1123-2020>
- Liu, X., Chen, F., Barlage, M., Zhou, G., & Niyogi, D. (2016). Noah-MP-Crop: Introducing dynamic crop growth in the Noah-MP land surface model. *Journal of Geophysical Research: Atmospheres*, 121(23), 13–953. <https://doi.org/10.1002/2016JD025597>
- Lokupitiya, E., Denning, S., Paustian, K., Baker, I., Schaefer, K., Verma, S., et al. (2009). Incorporation of crop phenology in Simple Biosphere Model (SiBcrop) to improve land-atmosphere carbon exchanges from croplands. *Biogeosciences*, 6(6), 969–986. <https://doi.org/10.5194/bg-6-969-2009>

- Lombardozi, D., Bonan, G., Wieder, W., Grandy, A., Morris, C., & Lawrence, D. (2018). Cover crops may cause winter warming in snow-covered regions. *Geophysical Research Letters*, 45(18), 9889–9897. <https://doi.org/10.1029/2018gl079000>
- Lombardozi, D. L., Lu, Y., Lawrence, P. J., Lawrence, D. M., Swenson, S., Oleson, K. W., et al. (2020). Simulating agriculture in the Community Land Model version 5. *Journal of Geophysical Research: Biogeosciences*, 125(8), e2019JG005529. <https://doi.org/10.1029/2019jg005529>
- Lu, D., & Ricciuto, D. (2019). Efficient surrogate modeling methods for large-scale Earth system models based on machine-learning techniques. *Geoscientific Model Development*, 12(5), 1791–1807. <https://doi.org/10.5194/gmd-12-1791-2019>
- Lu, D., Ricciuto, D., Stoyanov, M., & Gu, L. (2018). Calibration of the E3SM land model using surrogate-based global optimization. *Journal of Advances in Modeling Earth Systems*, 10(6), 1337–1356. <https://doi.org/10.1002/2017ms001134>
- Ma, B., & Dwyer, L. (2001). Maize kernel moisture, carbon and nitrogen concentrations from silking to physiological maturity. *Canadian Journal of Plant Science*, 81(2), 225–232. <https://doi.org/10.4141/p00-073>
- McDermid, S., Mearns, L., & Ruane, A. (2017). Representing agriculture in Earth system models: Approaches and priorities for development. *Journal of Advances in Modeling Earth Systems*, 9(5), 2230–2265. <https://doi.org/10.1002/2016ms000749>
- Moore, C. E., Berardi, D. M., Blanc-Betes, E., Dracup, E. C., Egenriether, S., Gomez-Casanovas, N., et al. (2020). The carbon and nitrogen cycle impacts of reverting perennial bioenergy switchgrass to an annual maize crop rotation. *GCB Bioenergy*, 12(11), 941–954. <https://doi.org/10.1111/gcbb.12743>
- Moore, C. E., von Haden, A. C., Burnham, M. B., Kantola, I. B., Gibson, C. D., Blakely, B. J., et al. (2021). Ecosystem-scale biogeochemical fluxes from three bioenergy crop candidates: How energy sorghum compares to maize and miscanthus. *GCB Bioenergy*, 13(3), 445–458. <https://doi.org/10.1111/gcbb.12788>
- Mueller, N. D., Butler, E. E., McKinnon, K. A., Rhines, A., Tingley, M., Holbrook, N. M., & Huybers, P. (2016). Cooling of US Midwest summer temperature extremes from cropland intensification. *Nature Climate Change*, 6(3), 317–322. <https://doi.org/10.1038/nclimate2825>
- Oleson, K., Lawrence, D., Bonan, G., Drewniak, B., Huang, M., Koven, C., et al. (2013). *Technical description of version 4.5 of the Community Land Model (CLM)*, NCAR technical note: NCARTN-503+STR. National Center for Atmospheric Research (NCAR). <https://doi.org/10.5065/D6R1W7M>
- Osborne, T., Gornall, J., Hooker, J., Williams, K., Wiltshire, A., Betts, R., & Wheeler, T. (2015). JULES-crop: A parametrisation of crops in the Joint UK Land Environment Simulator. *Geoscientific Model Development*, 8(4), 1139–1155. <https://doi.org/10.5194/gmd-8-1139-2015>
- Popp, A., Calvin, K., Fujimori, S., Havlik, P., Humpenöder, F., Stehfest, E., et al. (2017). Land-use futures in the shared socio-economic pathways. *Global Environmental Change*, 42, 331–345. <https://doi.org/10.1016/j.gloenvcha.2016.10.002>
- Qian, Y., Wan, H., Yang, B., Golaz, J.-C., Harrop, B., Hou, Z., et al. (2018). Parametric sensitivity and uncertainty quantification in the version 1 of E3SM atmosphere model based on short perturbed parameter ensemble simulations. *Journal of Geophysical Research: Atmospheres*, 123(23), 13–046. <https://doi.org/10.1029/2018jd028927>
- Ricciuto, D. (2022). Offline Land Model Testbed (OLMT). Retrieved from <https://github.com/dmricciuto/OLMT>
- Ricciuto, D., Sargsyan, K., & Thornton, P. (2018). The impact of parametric uncertainties on biogeochemistry in the E3SM land model. *Journal of Advances in Modeling Earth Systems*, 10(2), 297–319. <https://doi.org/10.1002/2017ms000962>
- Robertson, A. D., Whitaker, J., Morrison, R., Davies, C. A., Smith, P., & McNamara, N. P. (2017). A *Miscanthus* plantation can be carbon neutral without increasing soil carbon stocks. *GCB Bioenergy*, 9(3), 645–661. <https://doi.org/10.1111/gcbb.12397>
- Saltelli, A., Annoni, P., Azzini, I., Campolongo, F., Ratto, M., & Tarantola, S. (2010). Variance based sensitivity analysis of model output. Design and estimator for the total sensitivity index. *Computer Physics Communications*, 181(2), 259–270. <https://doi.org/10.1016/j.cpc.2009.09.018>
- Sargsyan, K. (2017). Surrogate models for uncertainty propagation and sensitivity analysis. In R. Ghanem, D. Higdon, & H. Owhadi (Eds.), *Handbook of uncertainty quantification*. Springer.
- Sargsyan, K., Safta, C., Najm, H., Debusschere, B., Ricciuto, D., & Thornton, P. (2014). Dimensionality reduction for complex models via Bayesian compressive sensing. *International Journal for Uncertainty Quantification*, 4(1), 63–93. <https://doi.org/10.1615/Int.J.UncertaintyQuantification.2013006821>
- Searchinger, T., Heimlich, R., Houghton, R. A., Dong, F., Elobeid, A., Fabiosa, J., et al. (2008). Use of US croplands for biofuels increases greenhouse gases through emissions from land-use change. *Science*, 319(5867), 1238–1240. <https://doi.org/10.1126/science.1151861>
- Seguin, B., Arrouays, D., Balesdent, J., Soussana, J.-F., Bondeau, A., Smith, P., et al. (2007). Moderating the impact of agriculture on climate. *Agricultural and Forest Meteorology*, 142(2–4), 278–287. <https://doi.org/10.1016/j.agrformet.2006.07.012>
- Shi, M., Fisher, J. B., Brzostek, E. R., & Phillips, R. P. (2016). Carbon cost of plant nitrogen acquisition: Global carbon cycle impact from an improved plant nitrogen cycle in the Community Land Model. *Global Change Biology*, 22(3), 1299–1314. <https://doi.org/10.1111/gcb.13131>
- Skinner, R. H., & Adler, P. R. (2010). Carbon dioxide and water fluxes from switchgrass managed for bioenergy production. *Agriculture, Ecosystems & Environment*, 138(3–4), 257–264. <https://doi.org/10.1016/j.agee.2010.05.008>
- Smith, C. M., David, M. B., Mitchell, C. A., Masters, M. D., Anderson-Teixeira, K. J., Bernacchi, C. J., & DeLucia, E. H. (2013). Reduced nitrogen losses after conversion of row crop agriculture to perennial biofuel crops. *Journal of Environmental Quality*, 42(1), 219–228. <https://doi.org/10.2134/jeq2012.0210>
- Sobol, I. M. (2001). Global sensitivity indices for nonlinear mathematical models and their Monte Carlo estimates. *Mathematics and Computers in Simulation*, 55(1–3), 271–280. [https://doi.org/10.1016/s0378-4754\(00\)00270-6](https://doi.org/10.1016/s0378-4754(00)00270-6)
- Song, Y., Jain, A., & McIsaac, G. (2013). Implementation of dynamic crop growth processes into a land surface model: Evaluation of energy, water and carbon fluxes under corn and soybean rotation. *Biogeosciences*, 10(12), 8039–8066. <https://doi.org/10.5194/bg-10-8039-2013>
- Song, Y., Jain, A. K., Landuyt, W., Khesghi, H. S., & Khanna, M. (2015). Estimates of biomass yield for perennial bioenergy grasses in the USA. *BioEnergy Research*, 8(2), 688–715. <https://doi.org/10.1007/s12155-014-9546-1>
- Tarantola, A. (2005). *Inverse problem theory and methods for model parameter estimation*. SIAM.
- Tian, S., Cacho, J. F., Youssef, M. A., Chescheir, G. M., & Nettles, J. E. (2015). Switchgrass growth and morphological changes under established pine-grass agroforestry systems in the lower coastal plain of North Carolina, United States. *Biomass and Bioenergy*, 83, 233–244. <https://doi.org/10.1016/j.biombioe.2015.10.002>
- Trócsányi, Z. K., Fieldsend, A., & Wolf, D. (2009). Yield and canopy characteristics of switchgrass (*Panicum virgatum* L.) as influenced by cutting management. *Biomass and Bioenergy*, 33(3), 442–448. <https://doi.org/10.1016/j.biombioe.2008.08.014>
- Van Esbroeck, G., Hussey, M., & Sanderson, M. (2003). Variation between Alamo and Cave-in-Rock switchgrass in response to photoperiod extension. *Crop Science*, 43(2), 639–643. <https://doi.org/10.2135/cropsci2003.6390>
- Verge, X., De Kimpe, C., & Desjardins, R. (2007). Agricultural production, greenhouse gas emissions and mitigation potential. *Agricultural and Forest Meteorology*, 142(2–4), 255–269. <https://doi.org/10.1016/j.agrformet.2006.06.011>
- Wu, X., Vuichard, N., Ciais, P., Viovy, N., Noblet-Ducoudré, N. D., Wang, X., et al. (2016). ORCHIDEE-CROP (v0), a new process-based agro-land surface model: Model description and evaluation over Europe. *Geoscientific Model Development*, 9(2), 857–873. <https://doi.org/10.5194/gmd-9-857-2016>

- Yazaki, Y., Mariko, S., & Koizumi, H. (2004). Carbon dynamics and budget in a *Miscanthus sinensis* grassland in Japan. *Ecological Research*, 19(5), 511–520. <https://doi.org/10.1111/j.1440-1703.2004.00665.x>
- Zeri, M., Anderson-Teixeira, K., Hickman, G., Masters, M., DeLucia, E., & Bernacchi, C. J. (2011). Carbon exchange by establishing biofuel crops in Central Illinois. *Agriculture, Ecosystems & Environment*, 144(1), 319–329. <https://doi.org/10.1016/j.agee.2011.09.006>
- Zeri, M., Hussain, M. Z., Anderson-Teixeira, K. J., DeLucia, E., & Bernacchi, C. J. (2013). Water use efficiency of perennial and annual bioenergy crops in Central Illinois. *Journal of Geophysical Research: Biogeosciences*, 118(2), 581–589. <https://doi.org/10.1002/jgrg.20052>
- Zhu, P., Zhuang, Q., Eva, J., & Bernacchi, C. (2017). Importance of biophysical effects on climate warming mitigation potential of biofuel crops over the conterminous United States. *Gcb Bioenergy*, 9(3), 577–590. <https://doi.org/10.1111/gcbb.12370>